Developmental Biology 437 (2018) 152–162

Contents lists available at ScienceDirect

Developmental Biology

journal homepage: www.elsevier.com/locate/developmentalbiology

Hypomorphic Smo mutant with inefficient ciliary enrichment disrupts the highest level of vertebrate Hedgehog response

Eduardo D. Gigante[a,b,1], Alyssa Bushey Long[b,1], Johanna Ben-Ami[b,c,2], Tamara Caspary[b,*]

[a] Neuroscience Graduate Program, Emory University, Atlanta, GA 30322, USA
[b] Department of Human Genetics, Emory University, Atlanta, GA 30322, USA
[c] Emory College of Arts and Sciences, Emory University, Atlanta, GA 30322, USA

ARTICLE INFO

Keywords:
Smoothened
Sonic hedgehog signaling
Primary cilia
Mouse development

ABSTRACT

Smoothened (Smo) is the essential transducer of Sonic hedgehog (Shh) signaling, which regulates cell fate and proliferation during embryogenesis. We identified a novel mouse mutant, *cabbie* (*cbb*), and found that its cause is a missense mutation in *Smo*. We showed the Smo^{cbb} mutation is insensitive to the Shh agonist SAG, perhaps due to the disruption of SAG binding. We characterized Smo^{cbb} for defects in craniofacial and skeletal development, as well as neural tube patterning, and revealed Smo^{cbb} affected processes that require the highest levels of Shh activity. Smo is normally enriched in cilia upon Shh stimulation; however, we detected inefficient enrichment of Smo in Smo^{cbb} mutants whether we stimulated with Shh or SAG. Taken together, our data suggest that the highest levels of vertebrate Hedgehog signaling activity require efficient Smo ciliary enrichment.

1. Introduction

Hedgehog (Hh) signaling is essential for embryogenesis and tissue homeostasis (Briscoe and Therond, 2013; Ingham and McMahon, 2001). In vertebrates, there are three classes of Hh ligands: Sonic (Shh), Indian (Ihh), and Desert hedgehog (Dhh), all of which require the G protein-coupled receptor (GPCR) Smoothened (Smo) for signal transduction (Echelard et al., 1993; Krauss et al., 1993; Riddle et al., 1993; Zhang et al., 2001). In the absence of Hh ligand, the Hh receptor Patched1 (Ptch1) inhibits Smo, which results in the downstream Gli transcription factors being cleaved to transcriptional repressors. Upon binding of Hh ligand to Ptch1, the inhibition is lost, leading to Smo activation and downstream signaling. The activation of Smo involves multiple steps that include conformational change, phosphorylation (Chen et al., 2011; Meloni et al., 2006; Chen et al., 2004), and ciliary enrichment (Chen et al., 2011; Eggenschwiler et al., 2001; Milenkovic et al., 2009; Boehlke et al., 2010). The processes that regulate Smo activation are part of the mechanism by which the level of Hh response is regulated for specific biological processes. Too much Hh leads to tumorigenesis, whereas too little leads to birth defects, including skeletal and craniofacial anomalies (Bale and Yu, 2001; Hatten and Roussel, 2011; Muenke and Beachy, 2000; Nanni et al., 1999; Roessler et al., 1996; Roessler et al., 1997; Vorechovsky et al., 1997; Wolter et al., 1997).

In vertebrates, primary cilia, the solitary microtubule-based projections found on virtually all cell types, are required for Hh signal transduction (Huangfu et al., 2003). Cilia are built and maintained via intraflagellar transport, which uses kinesin and dynein motors for anterograde and retrograde traffic, respectively. The core Hh pathway components traffic dynamically in and out of cilia in a Hh ligand-dependent manner. In the absence of Shh, Ptch1 is visible in cilia (Rohatgi et al., 2007). Upon stimulation with Shh, Ptch1 becomes undetectable in cilia, whereas Smo is enriched (Corbit et al., 2005). This enrichment, while not sufficient for Smo activation, is considered a necessary step in activating Smo (Rohatgi et al., 2009).

Smo is a 7-transmembrane domain GPCR characterized by a large cysteine-rich domain (CRD) at its amino terminus, which plays an essential role in Smo dimerization and function (Zhao et al., 2007). The Smo CRD is known to associate with sterols, and recent evidence shows cholesterol can directly activate Smo, consistent with the findings that impaired cholesterol synthesis in Smith-Lemli-Opitz syndrome impairs Smo activation (Blassberg et al., 2016; Huang et al., 2016; Luchetti et al., 2016; Xiao et al., 2017). However, the exact processes involved in activation of Smo remain uncharacterized. Methods to measure Smo activation have been limited to downstream processes such as Smo phosphorylation (Chen et al., 2011; Meloni et al., 2006; Chen et al.,

* Corresponding author.
E-mail addresses: eduardo.gigante@emory.edu (E.D. Gigante), abushey@emory.edu (A.B. Long), jbenami1@pride.hofstra.edu (J. Ben-Ami), tcaspar@emory.edu (T. Caspary).
[1] These authors contributed equally
[2] Present address: Donald and Barbara Zucker School of Medicine at Hofstra/Northwell, Hempstead, NY 11549, USA

https://doi.org/10.1016/j.ydbio.2018.03.019
Received 17 November 2017; Received in revised form 4 March 2018; Accepted 20 March 2018
Available online 20 March 2018
0012-1606/

2004), trafficking (Eggenschwiler et al., 2001; Milenkovic et al., 2009; Kovacs et al., 2008), and transcriptional pathway output. Smo activation may involve its phosphorylation at multiple sites in its C-terminal tail, which induce a conformational change of Smo to an active state (Chen et al., 2011). It's unclear where this conformational change occurs, as there is evidence that Smo continuously cycles through the cilium (Ocbina and Anderson, 2008). Graded increases in Hh stimulation induce increasing amounts of phosphorylation carried out by several kinases, including PKA, CK1α, GRK2, and CK1γ (Chen et al., 2011; Li et al., 2016).

Smo has a heptahelical ligand-binding domain known to interact with several exogenous compounds that have helped us better understand Smo activation and how it relates to the primary cilium. For instance, Smoothened agonist (SAG) directly activates Smo, bypassing Ptch1-mediated inhibition, and enriches Smo in the cilium (Rohatgi et al., 2009; Chen et al., 2002; Frank-Kamenetsky et al., 2002). The exact mechanism of ciliary Smo enrichment involves several proteins, including β-arrestin and kinesin motors (Kovacs et al., 2008). In cells lacking cilia, SAG treatment induces partial phosphorylation of Smo, which can be blocked by inhibiting CK1α (Li et al., 2016).

In mice, loss of *Smo* is lethal just prior to embryonic day 9.5 (E9.5) since there is no transduction of signaling from Shh, Ihh, or Dhh (Zhang et al., 2001; Caspary et al., 2002). The roles of Shh and Ihh in processes like craniofacial and skeletal development as well as neural patterning stem largely from work on *Shh* or *Ihh* mutant mice. Shh signaling exerts a strong influence on craniofacial development, and small changes to the pathway output can dramatically alter the facial midline (Zaghloul and Brugmann, 2011). Between E9.5 and E10.5, Shh expression slowly increases in the pharyngeal endoderm, along the midline of the facial ectoderm, and in the ventral forebrain neuroectoderm (Jeong and McMahon, 2005). Here, Shh expression promotes neural crest cell survival and is essential for craniofacial organization, especially for structures in the midline. The olfactory placodes and nasal pits normally develop bilaterally in the ectoderm overlying the ventral forebrain. In embryos without *Smo* or *Shh*, a single nasal pit is located medially, indicating Hh signaling is required for proper craniofacial separation (Zhang et al., 2001; Caspary et al., 2002; Chiang et al., 1996). Loss of *Shh* disrupts the bilateral symmetry of facial development, resulting in defects such as cyclopia and holoprosencephaly; these defects are well documented in humans and mice (Roessler et al., 1996; Chiang et al., 1996; Belloni et al., 1996). Shh promotes the development of skeletal tissues of the limb buds and digits, spine, ribs, face, and skull (Chiang et al., 1996). At birth, the long bones of the forelimb (the humerus, radius, and ulna) are ossified, along with centers at the base of each digit. Ihh inhibits chondrocyte differentiation and instead supports bone ossification by promoting chondrocyte proliferation in cartilaginous tissues, and facilitates bone lengthening in the limbs at the growth plate (St-Jacques et al., 1999).

Shh plays a critical role in specifying the cell fates of neural progenitor cells in the developing neural tube (Chiang et al., 1996). Shh ligand is expressed in the notochord and produces a ventral-to-dorsal activity gradient that determines specific cell fates based on the level of Shh activity (Ericson et al., 1997). For example, the cells at the ventral midline of the neural tube experience the highest level of Shh activity and are specified as floor plate expressing FoxA2 and Shh (Briscoe et al., 2000). The cells adjacent to the floor plate express Nkx2.2, while the next adjacent domain expresses Olig2 (Briscoe et al., 1999; Lu et al., 2000). The level of Shh activity integrates the concentration and duration a progenitor cell is exposed to ligand (Dessaud et al., 2010; Dessaud et al., 2007; Ribes et al., 2010). *Smo* null mutants specify no ventral cell fates (Zhang et al., 2001; Caspary et al., 2002).

In this study, we reveal that an N-ethyl-N-nitrosourea (ENU)-induced mouse mutant, *cabbie* (*cbb*), is a novel allele of *Smo*. We identified *cbb* in the course of a forward genetic mouse screen for recessive mutations affecting embryonic neural development and picked up *cbb* due to the craniofacial defects we saw at E10.5. *cbb* mutants die shortly after birth. We show *cbb* embryos display defects that affect cells requiring the highest level of Shh activity. Furthermore, we find that the Smo protein in *cbb* mutants does not enrich properly in cilia. Taken together, our data argue that proper ciliary Smo enrichment is necessary for full Smo activation.

2. Materials and methods

2.1. Mice

All mice were cared for in accordance with NIH guidelines and Emory's Institutional Animal Care and Use Committee (IACUC). Alleles used were: Smo^{cbb} [MGI: 5911831], *Patched1-lacZ* [MGI: 1857447], and Smo^{bnb} [MGI: 2137553]. Genotyping was performed as previously published or as indicated below (Caspary et al., 2002; Goodrich et al., 1997). Timed matings of heterozygous intercrosses were performed to generate embryos of the indicated stage, with somite-matched pairs examined at each stage (E9.5, E10.5, E11.5). We saw no differences between wild-type or heterozygous Smo^{cbb} embryos and show the heterozygous phenotype as “control” throughout this report.

2.2. Mapping and identification of the cabbie mutation

The *cabbie* mutation was identified in a screen for recessive ENU mutations that caused morphological defects during midgestation. Induced on a C57BL/6 J background and backcrossed onto FVB/NJ, *cbb* was mapped to chromosome 6 using a low-density Illumina chip. The *cbb* mutation was refined to a 5-MB interval (D6Mit159 to D6Mit268) using SSLP marker-based PCR. Through whole-exome sequencing (Mouse Mutant Resequencing Project, Broad Institute) and subsequent analysis using SeqAnt, a cytosine-to-adenine SNP in exon 3 of the *Smoothened* (*Smo*) gene was identified (Shetty et al., 2010). Genotyping was performed by PCR using D6MIT159 primers (Fwd: 5’- CATATTCAAGACGGAGACTAGTTCC-3’, Rev: 5’-CACATGAAACACATGCACACA-3’) to amplify a strain-specific variation 3 kb upstream of the *cbb* point mutation. We confirmed the linkage of this marker via analysis of 225 E10.5 embryos from our breeding pedigree: 175/176 embryos phenotypically classified as normal genotyped as “control” (homozygous or heterozygous FVB at D6MIT159), and 49/49 embryos phenotypically classified as *cbb* genotyped as “mutant” (homozygous C57BL/6 at D6MIT159).

2.3. Phenotypic analysis of embryos and newborn pups

Embryos were dissected in cold phosphate-buffered saline and processed for β-galactosidase activity or immunofluorescence as previously described (Horner and Caspary, 2011). Antibodies used were: Shh, Nkx2.2 (Developmental Studies Hybridoma Bank; 1:5); FoxA2 (Cell Signaling; 1:500); Olig2 (Millipore; 1:300); Arl13b (NeuroMab 455-8JD-29; 1:500); Smo (kindly provided by K Anderson; 1:500); Alexa Fluor 488 and Alexa Fluor 568 (1:300, ThermoFisher); and Hoechst nuclear stain (1:3000). Alizarin red and alcian blue staining were performed as previously described (Caspary et al., 2007; Shen et al., 1997).

2.4. Mouse embryonic fibroblasts

Mouse embryonic fibroblasts (MEFs) were isolated and immortalized as previously described (Mariani et al., 2016). Control and Smo^{cbb} MEFs were grown on coverslips at a density of 0.5×10^6 cells/mL and treated for 24 h with 0.5% fetal bovine serum (FBS) Shh-conditioned medium (Larkins et al., 2011), 0.5% FBS medium containing 100 or 400 nM SAG (Millipore), 0.5% FBS medium containing 5 uM cyclopamine (Toronto Research Chemicals), or 0.5% FBS DMEM. Ten images

were taken of each coverslip and scored by two independent reviewers blinded to genotype. Smo localization in cilia was categorized as full, partial, or negative (Fig. 6A).

2.5. RT-qPCR analysis

Control and *Smo*^{cbb} MEFs were treated with Shh-conditioned or 0.5% FBS media every 24 h and harvested after 24, 48, or 72 h. RNA was isolated by QIAshredder homogenizer columns and RNeasy kit (Qiagen) following the manufacturer's instructions. cDNA was synthesized with iScript Reverse Transcription Supermix (Bio-Rad) using 200 ng of RNA per reaction following the manufacturer's instructions. Primers used were: *Ptch1* 5'-TGCTGTGCCTGTGGTCATCCTGATT-3', and 5'-CAGAGCGAGCATAGCCCTGTGGTTC-3'; *Gli1* 5'-CTTCACCCTGCCATGAAACT-3', and 5'-TCCAGCTGAGTGTTGTCCAG-3'; *Pold3* 5'-ACGCTTGACAGGAGGGGGCT-3', and 5'-AGGAGAAAAGCAGGGGCAAGCG-3' (Mariani et al., 2016). RT-qPCR reactions were performed in technical triplicate on three biological replicates as previously described. *Gli1* and *Ptch1* expression levels were normalized to the corresponding *Pold3* levels for each replicate. Normalized RT-qPCR data were analyzed by ANOVA with Bonferroni correction for multiple comparisons.

2.6. Structural prediction

The Smo protein structure was modeled using PyMol (Version 2.0; Python) and UCSF Chimera resource (version 1.12) (Pettersen et al., 2004). The mutation model was formed by 500 sequential iterations of energy minimization and geometry optimization on crystallized human Smo receptor bound to SAG ligand (PDB: 4QIN) (Wang et al., 2014).

3. Results

3.1. cabbie is a novel Smoothened allele

We identified the *cbb* mutation in a recessive ENU screen for embryos with abnormal morphology at E10.5. *cbb* embryos displayed a reduced frontonasal prominence (FNP), and the nasal pits collapsed towards the midline (Fig. 1A,B and Fig. 2A,B). We induced the *cbb* mutation on a C57BL/6 background and backcrossed to FVB so that we could use polymorphic markers and linkage analysis to map the *cbb* mutation. We found that *cbb* was located on chromosome 6. Through whole-exome sequencing, we identified a cytosine-to-adenine transversion in exon 3 of the *Smo* gene. The change is predicted to mutate a conserved asparagine (amino acid 223) to a lysine (Fig. 1C) at a position between the N-terminal cysteine-rich domain (CRD) and transmembrane domain 1 (Fig. 1D).

To determine whether the C→A mutation underlies the *cbb* phenotype, we performed a complementation test with a null allele of *Smo*: *bent body (bnb)* (Caspary et al., 2002; Kasarskis et al., 1998). *Smo*^{bnb} single mutant embryos display a distinct head shape, small body size, failed embryonic turning, and lethality just before E9.5 (Fig. 1G), whereas *Smo*^{cbb} single mutants survived until just after birth. At E9.5, *Smo*$^{cbb/bnb}$ embryos display a reduced FNP and first branchial arch (Fig. 1H). By E10.5, *Smo*$^{cbb/bnb}$ embryos were often small compared to control littermates (Fig. 1I,J). *Smo*$^{cbb/bnb}$ heteroallelic embryos died at E10.5–11.5, indicating that the alleles fail to complement and the C→A mutation is causative. Thus, the *Smo*$^{cbb/bnb}$ phenotype was less severe than the *Smo*$^{bnb/bnb}$ null phenotype, suggesting *Smo*^{cbb} is a hypomorphic allele of *Smo*.

3.2. Smo^{cbb} causes craniofacial and skeletal defects

To determine the functional consequences of the *Smo*^{cbb} allele, we examined craniofacial and skeletal development since both processes depend on Hh signaling. *Smo* null embryos display a single medially located nasal pit by E9.0, their point of lethality (Zhang et al., 2001; Caspary et al., 2002; Kasarskis et al., 1998). In contrast, *Smo*^{cbb} mutants were commonly indistinguishable from controls at E9.5 (Fig. 1F). By E10.5, *Smo*^{cbb} embryos display abnormal outgrowth of the nasal processes and a rotation of the nasal pits (Fig. 2A,B). The *Smo*^{cbb} phenotype progresses as development continues. At birth, *Smo*^{cbb} mutants display hypoplastic mandibles (Fig. 2 C-F), nasal and maxillary bones (Fig. 2G,H). These data suggest *Smo*^{cbb} permits Hh signaling, yet the highest level of response is not achieved, consistent with *Smo*^{cbb} being a hypomorphic allele.

We examined the skeletons of *Smo*^{cbb} embryos, where Shh and Ihh each play critical roles. Despite the craniofacial defect, we found many of the bones of the skull developed in the appropriate size and position (Fig. 2G,H). We saw that the long bones of *Smo*^{cbb} postnatal day 0 (P0) pups were shorter than those of littermate controls (Fig. 2I,J). In the caudal vertebral column, the centers of each vertebra ossify in the control pups (Fig. 2K,S); however, in the *Smo*^{cbb} pups, the vertebral bodies were barely present (Fig. 2L,T). In the limbs, we consistently saw digit defects across *Smo*^{cbb} pups, but the number of digits and presence of ossification centers varied in front- and hindlimb paws (Fig. 2O-R). In addition, the mandibles in *Smo*^{cbb} embryos were consistently smaller than littermate controls, but in some cases, we observed premature fusion at the symphysis (Fig. 2M,N). Such subtle phenotypic variability among *Smo*^{cbb} mutants is consistent with this being a hypomorphic allele affecting processes that require the highest levels of Hh signaling.

3.3. Smo^{cbb} mutant embryos display abnormal neural tube patterning

Neural cell fates in the embryonic neural tube depend on Shh activity (Chiang et al., 1996). To monitor Shh activity in the neural tube, we used a *Ptch1-lacZ* allele since *Ptch1* is a transcriptional target of Shh signaling (Goodrich et al., 1997). In the control neural tube at E10.5, we saw a steep ventral-to-dorsal gradient of lacZ staining, whereas in the neural tube of *Smo*^{cbb}, we saw a diminished lacZ gradient, indicating reduced Shh activity (Fig. 3A,B). To determine whether the reduced Shh activity led to changes in cell fate, we examined neural patterning in *Smo*^{cbb} embryos. We found Shh staining in the notochord of both control and *Smo*^{cbb} mutants at E10.5, suggesting the ligand is produced normally (Fig. 3C,D). At the ventral midline of the control neural tube, we observed Shh staining in the columnar cells of the floor plate (Fig. 3C); however, we detected few Shh-positive columnar cells in the *Smo*^{cbb} embryos, indicating a reduced floor plate (Fig. 3D). The floor plate is the secondary signaling center that produces Shh ligand (Ericson et al., 1997) and expresses FoxA2 (Fig. 3E). In E10.5 *Smo*^{cbb} mutants, we observed fewer FoxA2-positive cells, some co-expressing Nkx2.2 (Fig. 3F). The motor neuron precursors (Olig2-positive) are dorsally adjacent to the Nkx2.2 population (Fig. 3G). In *Smo*^{cbb} mutants, the Olig2 cells expanded ventrally, but not dorsally, compared to control neural tubes (Fig. 3H). Taken together, these data suggest that less Shh production in the floor plate leads to lowered Shh response at the ventral midline and the appropriate Shh response at the dorsal Olig2 boundary.

Progenitors in the neural tube are sensitive to both concentration and duration of Shh exposure (Dessaud et al., 2010; Dessaud et al., 2007; Ribes et al., 2010). To examine the possibility that *Smo*^{cbb} mutants might delay the kinetics of Smo activation leading to late cell fate specification in the neural tube, we examined neural tube patterning in E11.5 embryos. In control embryos at E11.5, we saw FoxA2-positive columnar cells in the floor plate and adjacent Nkx2.2- and Olig2-positive cells (Fig. 3I,K). In *Smo*^{cbb} mutants at E11.5, we observed few columnar cells expressing FoxA2 at the midline, which instead was populated by Nkx2.2-positive cells, indicating the floor plate remained unspecified. In contrast to E10.5 *Smo*^{cbb} mutants, we saw no coexpression of FoxA2 and Nkx2.2 (Fig. 3J). The Olig2 domain appeared adjacent to the Nkx2.2 domain in both control and *Smo*^{cbb}

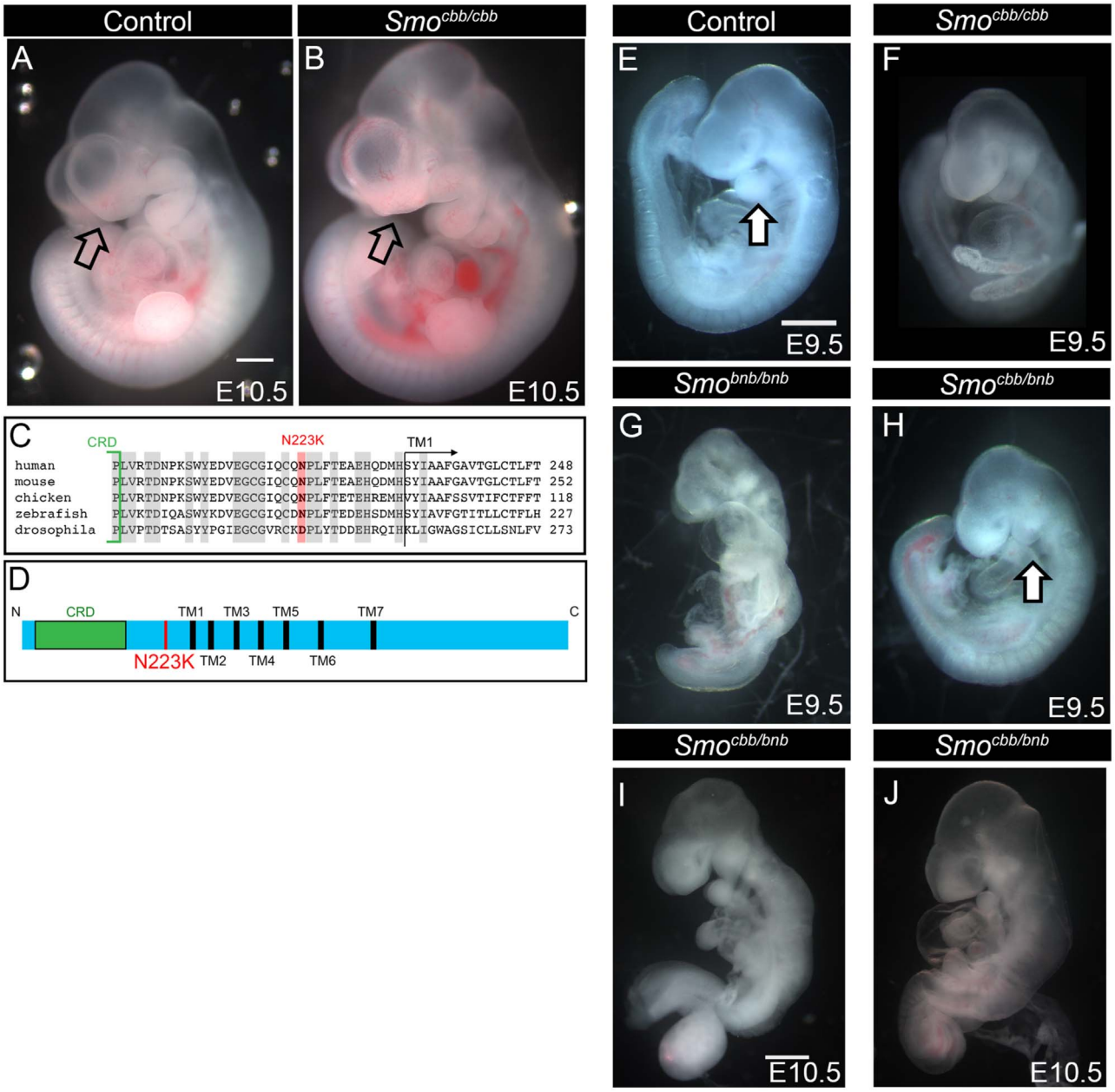

Fig. 1. *Smo*^{cbb} is a novel allele of *Smo*. (**A** and **B**) E10.5 control and *Smo*^{cbb} somite-matched embryos. Open arrows point to the FNP. (**C**) The *cbb* mutation changes a conserved asparagine residue to lysine; the species alignment shows the changed residue in red and conserved residues in gray. (**D**) Within the Smo protein, N223K (red) is located between the CRD (green) and transmembrane domain 1 (TM1, black). Somite-matched control (**E**) and *Smo*$^{cbb/cbb}$ (**F**) embryos at E9.5. The mutant embryo is nearly indistinguishable from control embryos at E9.5. Of 95 E9.5 embryos dissected: 9 were abnormal or dead, 61 were correctly identified as controls, 6 were correctly identified as *Smo*^{cbb} mutants, and 19 were called controls but genotyped as *Smo*^{cbb}. (**G**) *Smo*^{bnb} embryos (null allele) are small with a distinct head shape, small somites, and incomplete embryonic turning. (**H**) *Smo*$^{cbb/bnb}$ E9.5 embryo. *Smo*^{cbb} fails to complement *Smo*^{bnb}. Filled arrows in (**E**) and (**H**) point to branchial arch 1. (**I** and **J**) At E10.5, *Smo*$^{cbb/bnb}$ embryos are viable, but phenotypically delayed with some variability in head size, cardioedema, branchial arch development, and viability. Scale bars are 500 μm.

mutants (Fig. 3K,L). Together, these data argue that *Smo*^{cbb} has disrupted the highest levels of Shh activity, and this disruption is not restored over time.

3.4. *In vitro analysis of Shh-dependent transcriptional targets in cultured mutant fibroblasts*

To directly examine the level of Shh response, we derived and immortalized mouse embryonic fibroblasts (MEFs) from *Smo*^{cbb} and control littermates. We measured transcription of the Shh target genes *Ptch1* and *Gli1* in the absence and presence of Shh. In control MEFs, we found increased *Gli1* and *Ptch1* expression 24 hours after treatment with Shh (Fig. 4A, black comparisons); however, we detected a significantly lower response in stimulated *Smo*^{cbb} MEFs, indicating that the Smo^{N223K} mutation impaired Shh signal transduction (Fig. 4A, red comparisons).

The reduced *Ptch1* and *Gli1* transcription we saw in the *Smo*^{cbb} MEFs upon Shh stimulation could reflect the moderate level of Shh activity seen in the embryo. Because the duration of Shh activity during development plays a key role in neural cell fate and digit specification, another possibility is that the Smo^{N223K} mutant has altered signal transduction kinetics (Dessaud et al., 2010; Dessaud et al., 2007; Ribes et al., 2010; Scherz et al., 2007). To examine this possibility, we compared the Shh transcriptional response in control and *Smo*^{cbb}

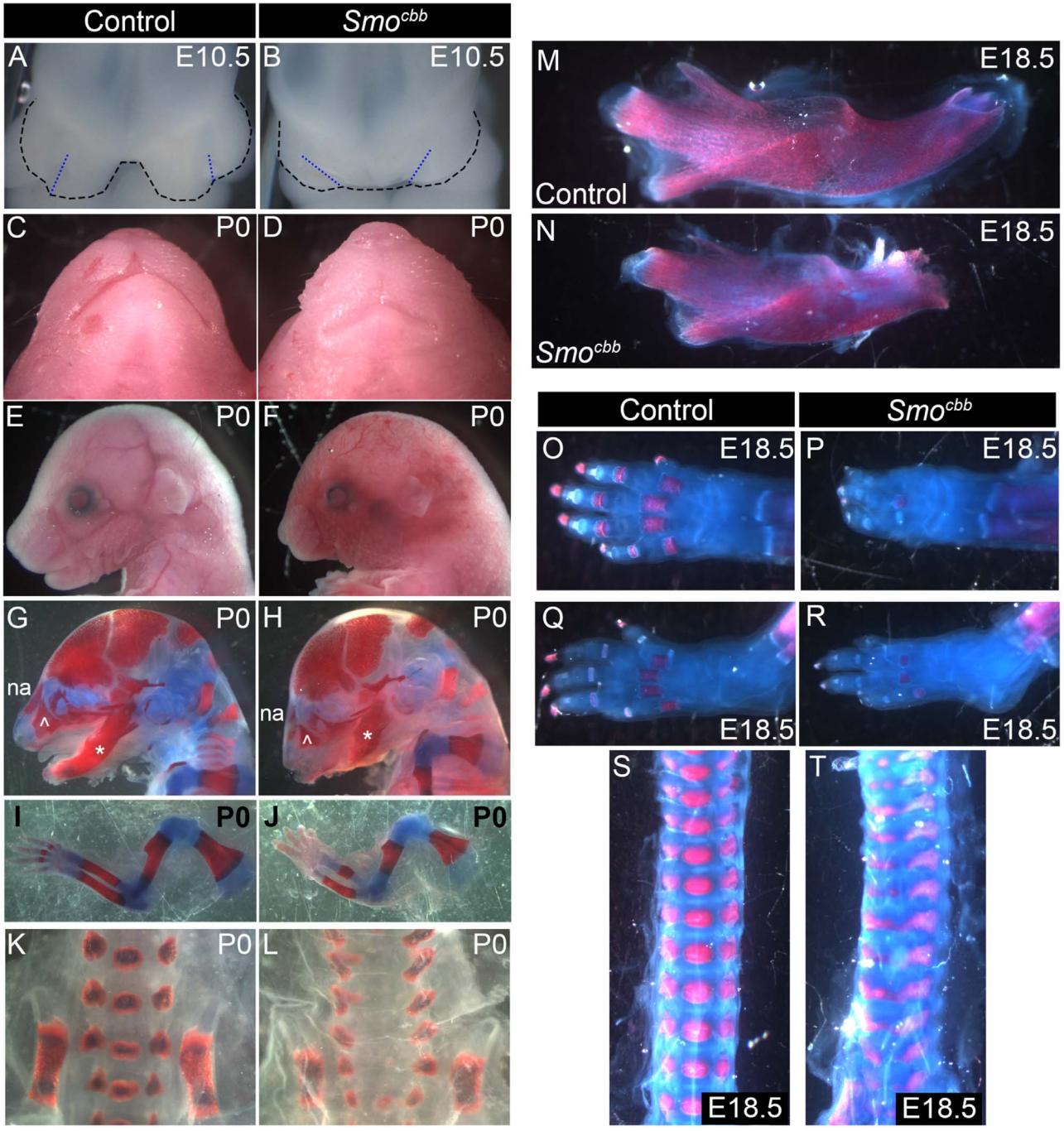

Fig. 2. Defective craniofacial and skeletal development in *Smo*^{cbb} mutants. (**A** and **B**) At E10.5, *Smo*^{cbb} mutants showed abnormal outgrowth of the nasal processes and a rotation of the nasal pits. n = 176 control and 54 *Smo*^{cbb} embryos. (**C** and **D**) By P0, *Smo*^{cbb} mutants displayed a more posterior location of the mouth compared to control littermates and (**E** and **F**) a concomitant reshaping of the face, especially the lower jaw. (**G** and **H**) Skeletal preparations of P0 pups show the hypoplastic mandibles (*), nasal (na) and maxillary (^) bones in the *Smo*^{cbb} mutants. (**M** and **N**) Isolated mandibles from E18.5 pups stained with alcian blue and alizarin red. (**I** and **J**) The forelimbs of *Smo*^{cbb} mutants show shorter long bones and a lack of ossification (red staining) in the digits. (**O** and **P**) Higher magnification view of E18.5 front paws. (**Q** and **R**) Higher magnification view of E18.5 hind paws. (**K**, **L**, **S**, and **T**) Spinal columns from *Smo*^{cbb} animals show small or absent vertebral bodies. Paired images were taken at the same magnification.

MEFs at 24, 48, and 72 hours. For the 48- and 72-hour time points, we re-stimulated with fresh Shh-conditioned culture medium every 24 hours. As expected, we found Shh stimulation induced *Ptch1* and *Gli1* transcription in control MEFs at all three time points, with the highest activity at 48 hours (Fig. 4B). In contrast, we found *Smo*^{cbb} MEFs did not display higher levels of transcriptional response after longer exposure to Shh. Expression of *Ptch1* and *Gli1* remained unchanged across all three time points (Fig. 4C). These data suggest that the Smo^{N223K} mutation disrupts the full activation of Smo.

3.5. N223K disrupts the Smo ligand-binding pocket and SAG binding to Smo

The asparagine-to-lysine change at position 223 in the *Smo*^{cbb} allele is located within the linker domain of the protein, downstream of the cysteine-rich domain (CRD) and immediately prior to the beginning of transmembrane domain 1 (Fig. 5A,B). The corresponding residue in the human SMO receptor contributes to a ligand-binding pocket, where SMO agonists and antagonists bind. In fact, one solved crystal

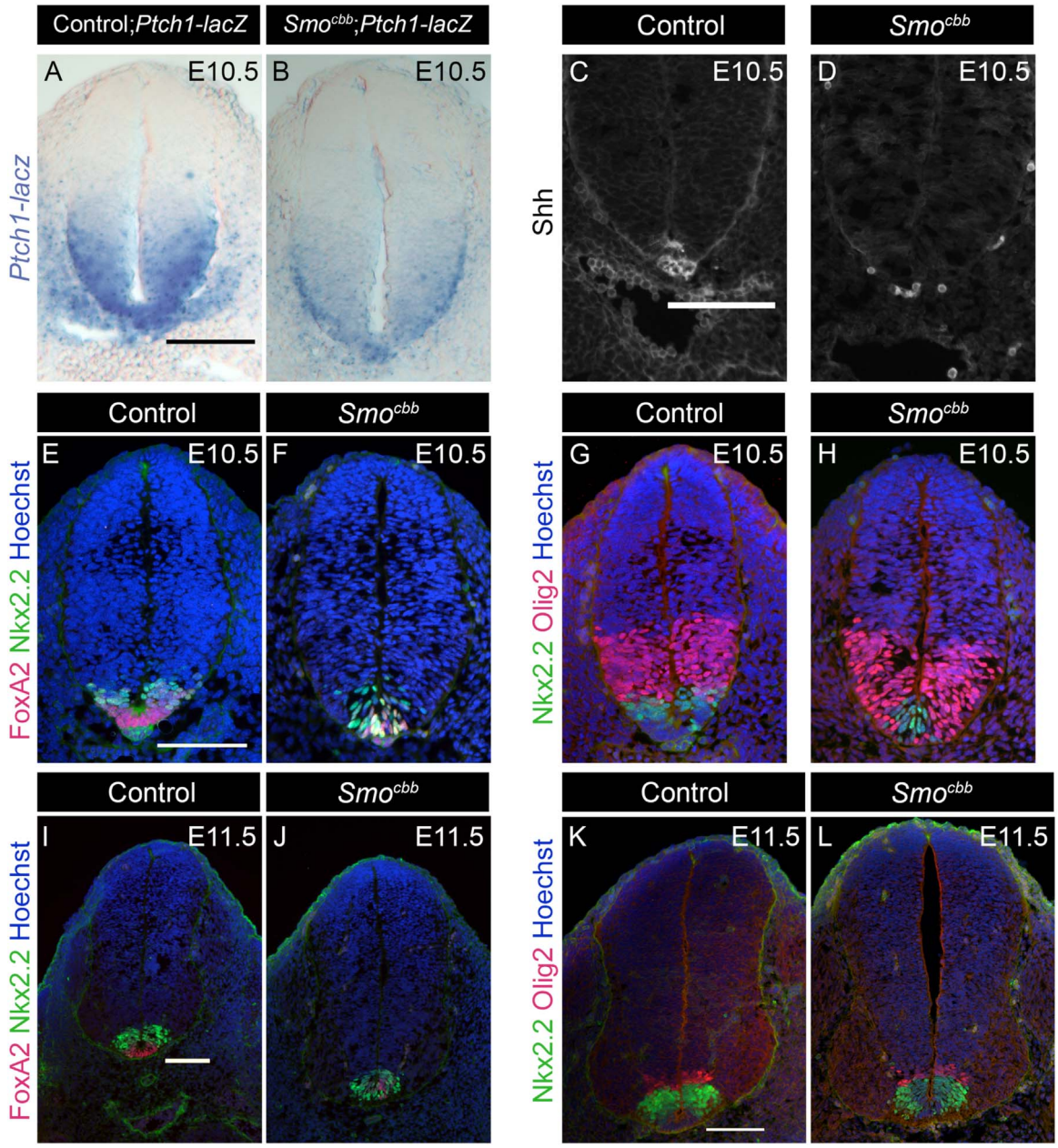

Fig. 3. Ventral shift of neural tube patterning in *Smo*^{cbb} mutant. (**A** and **B**) Ptch1-lacZ gradient in Control;*Ptch1-lacZ* and *Smo*^{cbb};*Ptch1-lacZ* neural tube sections. (**C** and **D**) Expression of Shh is greatly diminished or absent in *Smo*^{cbb}. (**E** and **F**) E10.5 and (**I** and **J**) E11.5 sections stained for FoxA2 (red) and Nkx2.2 (green). (**G** and **H**) E10.5 and (**K** and **L**) E11.5 sections stained for Olig2 (red) and Nkx2.2 (green). Images are axial sections of somite-matched embryos through hindlimb-level neural tube. Scale bars are 100 μm.

structure shows Smo agonist (SAG) associates with the ligand-binding pocket, and hydrogen bonds with the asparagine corresponding to N223 in the mouse protein (Wang et al., 2014; Wang et al., 2013). Based on the solved structure, we modeled the N223K mutation (N219K in human) and found that a change from asparagine to lysine is predicted to occlude the Smo binding pocket and interfere with the binding of SAG, a potent agonist (Fig. 5C,D), suggesting that Smo^{N223K} might be SAG-insensitive.

To test this directly, we treated control and *Smo*^{cbb} mutant MEFs with SAG and measured Shh transcriptional response. We detected increased *Ptch1* and *Gli1* expression in SAG-treated control MEFs compared to untreated cells (Fig. 5E, black comparisons). In contrast, we found *Smo*^{cbb} mutant MEFs were unresponsive to SAG treatment; we saw no change in *Gli1* or *Ptch1* expression, and the level of expression in SAG-treated *Smo*^{cbb} MEFs was statistically lower than in control MEFs (Fig. 5E, red comparisons). Next, we tested whether the *Smo*^{cbb} MEFs could respond to a higher dose of SAG (400 nM, four times higher than in the previous experiment). This dose was also ineffective at increasing Shh transcriptional response in mutant MEFs, suggesting the N223K mutation renders the Smo receptor refractory to SAG. (Fig. 5F). We note that while neither Shh nor SAG statistically induced *Gli1* or *Ptch1* expression, the slight response we detected in Shh-treated *Smo*^{cbb} MEFs may be biologically distinct from the lack of expression we saw in SAG-treated *Smo*^{cbb} MEFs (Figs. 4A,5E). Together, these data are consistent with the Smo^{N223K} mutation altering the ligand-binding pocket, such that SAG cannot effectively bind and activate the receptor.

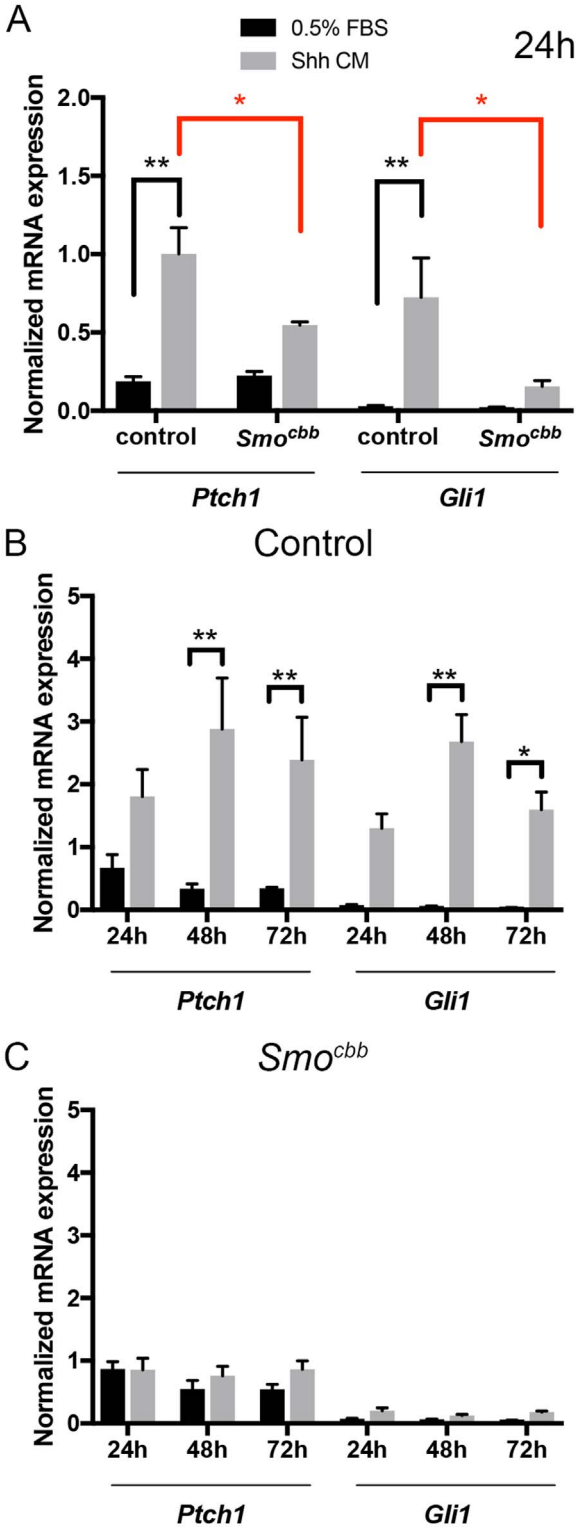

Fig. 4. Analysis of Shh target transcription in *Smo*^{cbb} MEFs. (**A**) Control MEFs showed robust induction of Shh transcriptional targets, *Ptch1* and *Gli1,* 24 hours after treatment with Shh-conditioned media (Shh CM), whereas *Smo*^{cbb} MEFs showed a small induction that did not reach statistical significance (black comparisons). The small expression levels of both *Ptch1* and *Gli1* in treated *Smo*^{cbb} MEFs were significantly reduced compared to Shh-treated control MEFs (red comparisons). (**B**) Control MEFs showed robust induction of Shh transcriptional targets, *Ptch1* and *Gli1,* 24, 48, and 72 hours after treatment with Shh-conditioned medium (reapplied every 24 hours), whereas *Smo*^{cbb} MEFs (**C**) showed a small induction that did not reach statistical significance. (**, $p < 0.001$; *, $p < 0.01$).

3.6. Smoothened localization defect in Smo^{cbb} *in vivo and in vitro after Shh and SAG activation*

In vertebrates, Smo is enriched in cilia upon pathway activation, a step that is necessary but not sufficient for Smo activation (Corbit et al., 2005; Rohatgi et al., 2009). We looked at Smo localization in relation to the primary cilium upon Shh stimulation in control and *Smo*^{cbb} MEFs. We examined ciliated cells and classified ciliary staining as fully Smo positive, partially Smo positive, or Smo negative (reviewers blinded to genotype, see Methods, Fig. 6A). In Shh-treated MEFs, we found 70% of control cilia were fully Smo positive, compared to 32% in *Smo*^{cbb} cilia (Fig. 6B). Similarly, in SAG-treated MEFs, we saw that 76% of control cells' cilia were fully Smo positive, compared to 34% of *Smo*^{cbb} cells' cilia (Fig. 6B). Smo antagonist cyclopamine leads to ciliary enrichment of Smo and binds deeper in the same binding pocket as SAG. In cyclopamine-treated cells, we saw 27% of *Smo*^{cbb} cilia were fully Smo positive compared to 32% in control MEFs (Fig. 6B). Moreover, we measured a decrease in baseline Smo localization in 0.5% FBS-treated *Smo*^{cbb} MEF cilia compared to controls, indicating an inherent defect in Smo^{N223K} enrichment (Fig. 6B). These data argue that ciliary enrichment of Smo was impaired in *Smo*^{cbb} MEFs, and the enrichment defect in *Smo*^{cbb} MEFs was the same whether we stimulated with a ligand that activates Smo through the endogenous pathway (Shh-conditioned media) or with pharmacological agents that drive ciliary enrichment of Smo (SAG and cyclopamine).

To investigate ciliary enrichment of Smo *in vivo,* we examined Smo localization in the E10.5 neural tube. We looked at ciliated cells of the floor plate (where Shh activity is normally at the highest levels) for co-localization of Smo and ciliary marker Arl13b. In the floor plate, where Shh signaling is highest in the neural tube, ~75% of cilia were Smo-positive in control sections compared to ~25% in *Smo*^{cbb} (Fig. 6C,D). These same cells express FoxA2 and Nkx2.2 cell fates in wild-type, whereas in *Smo*^{cbb} mutants they only express Nkx2.2 (Fig. 3E,F). Thus, Smo^{N223K} appears to remain present in cilia at the ventral neural tube, but at much lower levels compared to wild-type. In the context of our data showing that *Smo*^{cbb} mutants do not achieve the highest levels of Shh activity in the floor plate, these results indicate that efficient Smo ciliary enrichment is required for the highest levels of Shh response.

4. Discussion

Here, we identified a mouse mutant displaying craniofacial, skeletal, and neural tube patterning defects and showed the defects are due to a N223K mutation in the Smo protein. We characterized several phenotypes in *Smo*^{cbb} homozygous embryos consistent with loss of maximal Hh signaling, among them a narrow FNP, a reduced floor plate in the neural tube, and shortened long bones. The *Smo*^{cbb} allele failed to complement a *Smo*^{bnb} null allele, indicating that the N223K mutation in Smo is causative. The *Smo*$^{cbb/bnb}$ compound mutant phenotype was less severe than *Smo*^{bnb} null, yet more severe than *Smo*^{cbb}, suggesting a partial-loss-of-function allele. *Smo*^{cbb} embryos survive until birth, indicating Smo^{N223K} receptor functions sufficiently for gestation to proceed. In contrast, we detected no significant induction of Shh target gene transcription in *Smo*^{cbb} MEFs, which could mean the N223K mutation disrupts the ability of Smo to be fully activated. Consistent with this, we showed that Smo^{N223K} protein is inefficiently enriched in cilia upon Shh stimulation.

Within vertebrates, the *Smo*^{cbb} mutation, N223K, occurs at a conserved residue corresponding to N219 in human SMO (hSMO), which lies within a linker domain between the CRD of the N-terminus and the first transmembrane domain. This linker domain is thought to facilitate CRD association with extracellular loop 1 when bound to oxysterols and cholesterol, which in turn is critical for Smo regulation (Wang et al., 2014; Wang et al., 2013; Byrne et al., 2016). One proposed mechanism for this is via a cysteine-cysteine disulfide bond between the N-terminus and extracellular loop 1 mediated by residue

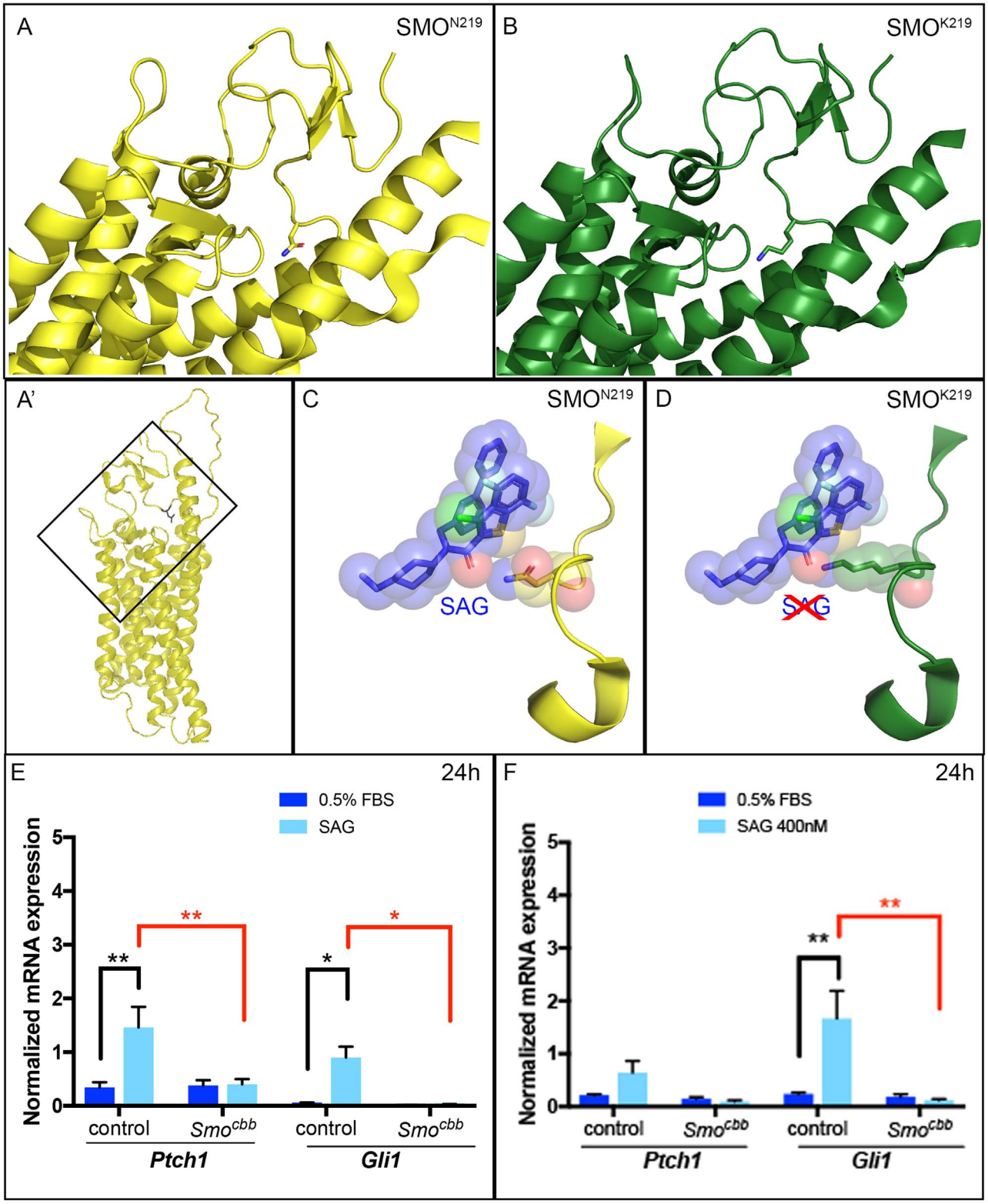

Fig. 5. The N223K mutation disrupts the Smo ligand-binding pocket and is insensitive to SAG. A three-dimensional ribbon model of the human SMO receptor with (**A**) asparagine or (**B**) predicted model with lysine at residue 219. (**A'**) Full model of human SMO receptor (aa194–557) with box representing the region of the molecule enlarged for clarity in (A) and (B). The membrane-spanning alpha helices are arranged so that the extra-cellular N-terminus of the protein is toward the top of the model. (**C**) N219 makes a hydrogen bond with Smo agonist (SAG; blue) as part of the ligand-binding pocket. (**D**) K219 is predicted to sterically clash with SAG, indicated by the crossed-out SAG. The ribbon backbone of SMO shown in (C) and (D) represents aa215–225, with the N-terminal end toward the top. (**E**) Control MEFs showed increased expression of *Ptch1* and *Gli1* after 24 hours of treatment with SAG, whereas Smo^{cbb} MEFs did not (black comparisons). Expression levels of both *Ptch1* and *Gli1* in treated Smo^{cbb} MEFs were reduced compared to SAG-treated controls (red comparisons). (**F**) Treatment with 400 nM SAG was unable to direct expression of *Ptch1* or *Gli1* in Smo^{cbb} MEFs. (**, $p < 0.001$; *, $p < 0.01$).

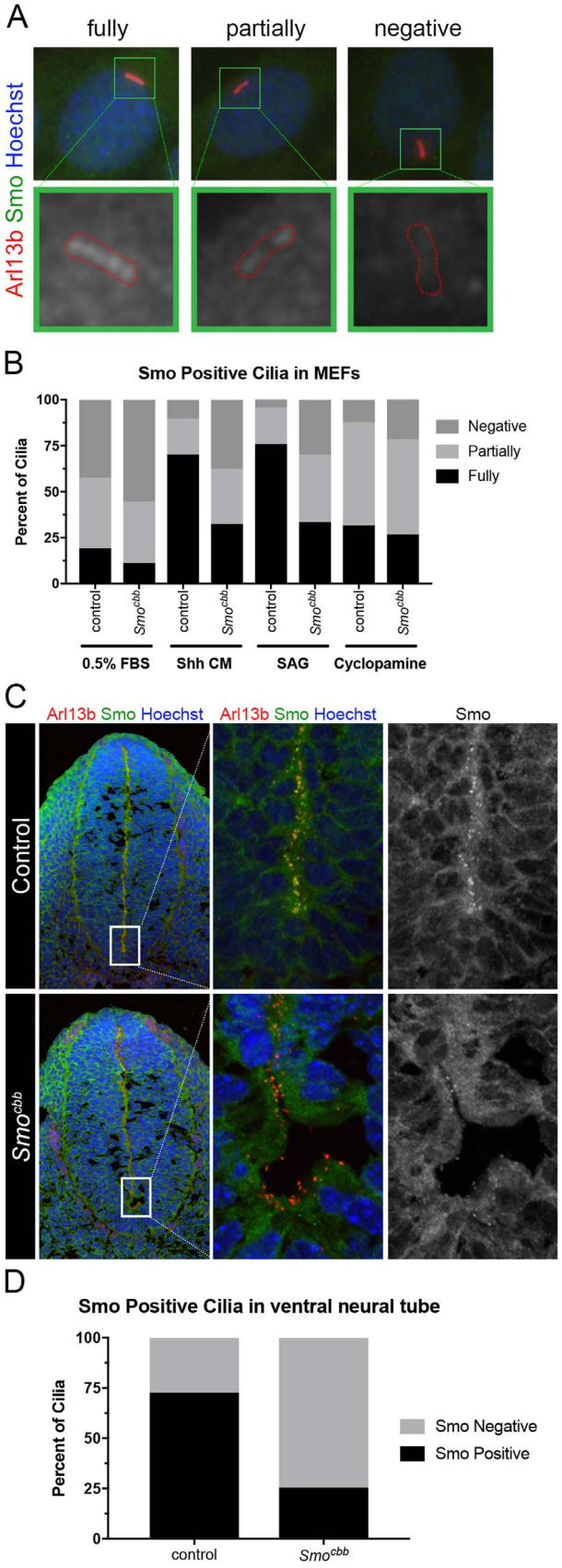

Fig. 6. Smo^{N223K} causes a cilia localization defect in MEFs and E10.5 neural tube. (**A**) Ciliary staining of Smo (green) in cilia (Arl13b; red) is classified as fully Smo positive, partially Smo positive, or Smo negative. The green channels of the top row insets are presented enlarged in the bottom row. Images are of monolayer MEFs on cover slip at 40×. (**B**) Quantification of Smo localization in control and Smo^{cbb} MEFs treated with

C217 in hSMO (Wang et al., 2013). Residue N219 in hSMO forms a critical hydrogen bond with SAG as part of the ligand-binding pocket. Without SAG, N219 forms two hydrogen bonds with L221 and D384 on extracellular loop 2. When bound to SAG, N219 releases its D384 bond and instead binds the SAG molecule, forming a lid on the ligand-binding pocket (Wang et al., 2014). In a simulation of human SMO N219K (Fig. 5), the L221 bond is lost, and only the D384 association remains, which may disrupt SAG binding. Alternatively, lysine is a larger residue than asparagine and is predicted to structurally interfere with the binding of SAG. A lack of SAG binding with Smo^{N223K} is consistent with the lack of SAG-induced gene transcription in Smo^{cbb} upon SAG treatment. Nevertheless, we do see some SAG-induced Smo enrichment in cilia; therefore, it is also possible that SAG binds Smo^{N223K}, and the downstream phenotypes we saw are due to a conformational change of Smo^{N223K}. When MEFs were treated with antagonist cyclopamine, we saw similar levels of Smo ciliary enrichment in both Smo^{cbb} and control MEFs. Cyclopamine is not known to associate with N223 when binding to Smo, and it is therefore unlikely that N223K alters cyclopamine binding directly (Chen et al., 2002; Chen et al., 2002). However, because N223 is located at the entrance of the ligand-binding pocket, N223K could interrupt the entry of cyclopamine. Because Smo^{cbb} MEFs do not transduce Shh-dependent genes in response to Shh or SAG, we cannot determine whether cyclopamine can antagonize the Smo^{N223K} receptor and block Shh gene transcription.

One of the most striking results in our studies was the fact that Smo^{cbb} embryos survived to birth, implying some Hh transduction; however, Smo^{cbb} MEFs did not display a statistically significant transcriptional response upon Shh stimulation, even after 72 hours of treatment (Fig. 4). One interpretation of these data is that the induction we saw in Smo^{cbb} MEFs, while not statistically significant, is biologically significant. Consistent with this interpretation is the fact that we saw no induction of *Gli1* or *Ptch1* transcription when we stimulated the Smo^{cbb} MEFs with moderate or high doses of SAG (Fig. 5C,D). If this interpretation is correct, then the time course in MEFs would mean that the N223K mutation disrupts the actual activation status of Smo, as opposed to the kinetics of its activation. Of course, the alternative explanation is that MEFs *in vitro* do not reflect what occurs in the living embryo *in vivo*.

Our work *in vivo* provided an unexpected finding about the level of Shh signaling in the notochord. The notochord is the source of the Shh morphogen, which is why this is where the highest concentration of ligand is seen (Echelard et al., 1993; Riddle et al., 1993). Previous work showed that the notochord degenerates in the absence of Smo, arguing that Shh signaling is required to maintain the notochord (Caspary et al., 2002). Our analysis of Smo^{cbb} mutants showed that the notochord was intact, but the floor plate was not properly specified, along with a clear deficit in Smo-positive cilia in the ventral floor plate. These data suggest that the floor plate, but not the notochord, requires the highest level of Shh signaling.

The reduced floor plate in Smo^{cbb} mutants appears to produce less Shh ligand than in controls. In the improperly specified Smo^{cbb} floor plate, we observed some Nkx2.2 and FoxA2 co-expressing cells, suggesting that cell identity is poorly defined at this stage. However, at E11.5, we noted a lack of co-labeled cells, suggesting that cell fates resolve over time. This indicates that Shh signal integration is delayed, but it does occur. That said, the simple model of neural patterning would predict that fewer floor plate cells expressing less Shh would lead to patterning defects in all the ventral cell fates. In fact, we observed the ventral expansion of Nkx2.2 and Olig2 fates but the dorsal position of the Olig2 domain was the same as in controls. This is reminiscent of *Gli2* mutants, which also do not specify a floor plate, but display a ventral expansion of intermediate cell fates and maintain the dorsal position of the Olig2 domain (Ding et al., 1998; Matise et al., 1998). Thus, the highest levels of Shh response appear necessary exclusively at the ventral midline of the neural tube.

In *Smo*^{cbb} mutants, the reduced floor plate, the lack of vertebral bodies in the backbone, the shortening of the long bones of the limbs, and the rotated nasal pits, all reflect a loss of the highest levels of Shh activity. In fact, the skeletal phenotype closely resembles that of the *Gli2* null embryo that shares late gestational lethality (Mo et al., 1997), further supporting a loss of high-level Shh. While recent evidence suggests that Smo activation can occur in a cilia-independent manner, the highest levels of activation appear to depend upon ciliary enrichment (Fan et al., 2014). Our finding that Smo^{N223K} is inefficiently trafficked to cilia suggests a model whereby the N223K mutation disrupts efficient protein trafficking to the cilium. The survival of *Smo*^{cbb} pups to birth argues that signaling is partially intact. The fact that SAG treatment has no impact on the ciliary enrichment of mutant Smo^{N223K} protein fits in well with both our proposal that SAG cannot bind Smo^{N223K} and the notion that phosphorylation of Smo outside the cilium initiates the switch of Smo to an active state. Smo is trafficked to cilia after the initial activation event that likely causes a change in its conformation in order to expose the C-terminal tail that is required for its ciliary enrichment (Corbit et al., 2005). G protein-coupled receptor associated sorting protein 2 (Gprasp2) interacts with the Smo C-terminus in addition to a protein, Pitchfork, in a complex that contains the kinesin Kif3b motor subunit (Jung et al., 2016). Additional evidence showing that β-arrestin binds Smo and facilitates the recruitment of kinesin motor Kif3a leads to a model whereby the whole complex is needed for Smo transport to the cilium (Kovacs et al., 2008). Future work is required to determine whether appropriate conformational changes occur in Smo^{N223K}, whether disulfide bonds that mediate the association between the sterol-bound CRD and the extracellular loop of Smo^{N223K} can be maintained, or whether the complexes that mediate ciliary trafficking form with Smo^{N223K}.

The overall conservation of the components and regulatory logic of Hh signaling, from flies through vertebrates, make the unique necessity of cilia for Hh signaling transduction in vertebrates particularly intriguing (Goetz and Anderson, 2010; Huangfu and Anderson, 2006). The *Smo*^{cbb} mutation may be a particularly relevant tool for understanding the relationship between Hh signaling and cilia in vertebrates because the poor Smo^{N223K} ciliary enrichment could represent a disruption specifically in the process co-opted by vertebrates for Hh regulation. At the most extreme end of interpretation, the *Smo*^{cbb} phenotype may reflect the evolutionarily conserved Hh mechanism, and it may be that to gain higher levels of Hh activity, another level of activation in the cilium evolved.

Acknowledgements

This work was supported by funding from NIH grants R01GM110663, R01NS090029, and R35GM122549 to T.C. E.D.G was supported by NIH training grant T32NS096050. Further support came from the Emory University Integrated Cellular Imaging Microscopy Core of the Emory Neuroscience NINDS Core Facilities grant, P30NS055077, as well as the Mouse Mutant Re-sequencing Project at the Broad Institute funded by NHGRI under grant U54 HG003067. We are grateful to Kajari Mondal, Viren Patel, and Michael Zwick for support using SeqAnt for the exome data, to Jennifer Colucci for support with PyMol modeling, to April Reedy at Emory's Integrated Cellular Imaging Core for assistance with confocal microscopy, to members of the Caspary lab for discussion and manuscript comments, and to Cheryl Timms Strauss for editing.

References

Briscoe, J., Therond, P.P., 2013. The mechanisms of Hedgehog signalling and its roles in development and disease. Nat Rev Mol Cell Biol **14** (7), 416–429.
Ingham, P.W., McMahon, A.P., 2001. Hedgehog signaling in animal development: paradigms and principles. Genes Dev **15** (23), 3059–3087.
Echelard, Y., et al., 1993. Sonic hedgehog, a member of a family of putative signaling molecules, is implicated in the regulation of CNS polarity. Cell **75** (7), 1417–1430.
Krauss, S., Concordet, J.P., Ingham, P.W., 1993. A functionally conserved homolog of the Drosophila segment polarity gene hh is expressed in tissues with polarizing activity in zebrafish embryos. Cell **75** (7), 1431–1444.
Riddle, R.D., et al., 1993. Sonic hedgehog mediates the polarizing activity of the ZPA. Cell **75** (7), 1401–1416.
Zhang, X.M., Ramalho-Santos, M., McMahon, A.P., 2001. Smoothened mutants reveal redundant roles for Shh and Ihh signaling including regulation of L/R symmetry by the mouse node. Cell **106** (2), 781–792.
Chen, Y., et al., 2011. Sonic Hedgehog dependent phosphorylation by CK1alpha and GRK2 is required for ciliary accumulation and activation of smoothened. PLoS Biol **9** (6), e1001083.
Meloni, A.R., et al., 2006. Smoothened signal transduction is promoted by G protein-coupled receptor kinase 2. Mol Cell Biol **26** (20), 7550–7560.
Chen, W., et al., 2004. Activity-dependent internalization of smoothened mediated by beta-arrestin 2 and GRK2. Science **306** (5705), 2257–2260.
Eggenschwiler, J.T., Espinoza, E., Anderson, K.V., 2001. Rab23 is an essential negative regulator of the mouse Sonic hedgehog signalling pathway. Nature **412** (6843), 194–198.
Milenkovic, L., Scott, M.P., Rohatgi, R., 2009. Lateral transport of Smoothened from the plasma membrane to the membrane of the cilium. J Cell Biol **187** (3), 365–374.
Boehlke, C., et al., 2010. Differential role of Rab proteins in ciliary trafficking: Rab23 regulates smoothened levels. J Cell Sci **123** (Pt 9), 1460–1467.
Bale, A.E., Yu, K.P., 2001. The hedgehog pathway and basal cell carcinomas. Hum Mol Genet **10** (7), 757–762.
Hatten, M.E., Roussel, M.F., 2011. Development and cancer of the cerebellum. Trends Neurosci **34** (3), 134–142.
Muenke, M., Beachy, P.A., 2000. Genetics of ventral forebrain development and holoprosencephaly. Curr Opin Genet Dev **10** (3), 262–269.
Nanni, L., et al., 1999. The mutational spectrum of the sonic hedgehog gene in holoprosencephaly: SHH mutations cause a significant proportion of autosomal dominant holoprosencephaly. Hum Mol Genet **8** (13), 2479–2488.
Roessler, E., et al., 1996. Mutations in the human Sonic Hedgehog gene cause holoprosencephaly. Nat Genet **14** (3), 357–360.
Roessler, E., et al., 1997. Mutations in the C-terminal domain of Sonic Hedgehog cause holoprosencephaly. Hum Mol Genet **6** (11), 1847–1853.
Vorechovsky, I., et al., 1997. Somatic mutations in the human homologue of Drosophila patched in primitive neuroectodermal tumours. Oncogene **15** (3), 361–366.
Wolter, M., et al., 1997. Mutations in the human homologue of the Drosophila segment polarity gene patched (PTCH) in sporadic basal cell carcinomas of the skin and primitive neuroectodermal tumors of the central nervous system. Cancer Res **57** (13), 2581–2585.
Huangfu, D., et al., 2003. Hedgehog signalling in the mouse requires intraflagellar transport proteins. Nature **426** (6962), 83–87.
Rohatgi, R., Milenkovic, L., Scott, M.P., 2007. Patched1 regulates hedgehog signaling at the primary cilium. Science **317** (5836), 372–376.
Corbit, K.C., et al., 2005. Vertebrate Smoothened functions at the primary cilium. Nature **437** (7061), 1018–1021.
Rohatgi, R., et al., 2009. Hedgehog signal transduction by Smoothened: pharmacologic evidence for a 2-step activation process. Proc Natl Acad Sci U S A **106** (9), 3196–3201.
Zhao, Y., Tong, C., Jiang, J., 2007. Hedgehog regulates smoothened activity by inducing a conformational switch. Nature **450** (7167), 252–258.
Blassberg, R., et al., 2016. Reduced cholesterol levels impair Smoothened activation in Smith-Lemli-Opitz syndrome. Hum Mol Genet **25** (4), 693–705.
Huang, P., et al., 2016. Cellular Cholesterol Directly Activates Smoothened in Hedgehog Signaling. Cell **166** (5), 1176–1187, e14.
Luchetti, G., et al., 2016. Cholesterol activates the G-protein coupled receptor Smoothened to promote Hedgehog signaling. Elife **5**, e20304.
Xiao, X., et al., 2017. Cholesterol Modification of Smoothened Is Required for Hedgehog Signaling. Mol Cell **66** (1), 154–162, e10.
Kovacs, J.J., et al., 2008. Beta-arrestin-mediated localization of smoothened to the primary cilium. Science **320** (5884), 1777–1781.
Ocbina, P.J., Anderson, K.V., 2008. Intraflagellar transport, cilia, and mammalian Hedgehog signaling: analysis in mouse embryonic fibroblasts. Dev Dyn **237** (8), 2030–2038.
Li, S., et al., 2016. Regulation of Smoothened Phosphorylation and High-Level Hedgehog Signaling Activity by a Plasma Membrane Associated Kinase. PLoS Biol **14** (6), e1002481.
Chen, J.K., et al., 2002. Small molecule modulation of Smoothened activity. Proc Natl Acad Sci U S A **99** (22), 14071–14076.
Frank-Kamenetsky, M., et al., 2002. Small-molecule modulators of Hedgehog signaling: identification and characterization of Smoothened agonists and antagonists. J Biol **1** (2), 10.
Caspary, T., et al., 2002. Mouse Dispatched homolog1 is required for long-range, but not juxtacrine, Hh signaling. Curr Biol **12** (18), 1628–1632.
Zaghloul, N.A., Brugmann, S.A., 2011. The emerging face of primary cilia. Genesis **49** (4), 231–246.
Jeong, J., McMahon, A.P., 2005. Growth and pattern of the mammalian neural tube are governed by partially overlapping feedback activities of the hedgehog antagonists patched 1 and Hhip1. Development **132** (1), 143–154.
Chiang, C., et al., 1996. Cyclopia and defective axial patterning in mice lacking Sonic hedgehog gene function. Nature **383** (6599), 407–413.
Belloni, E., et al., 1996. Identification of Sonic hedgehog as a candidate gene responsible for holoprosencephaly. Nat Genet **14** (3), 353–356.
St-Jacques, B., Hammerschmidt, M., McMahon, A.P., 1999. Indian hedgehog signaling regulates proliferation and differentiation of chondrocytes and is essential for bone

formation. Genes Dev **13** (16), 2072–2086.
Ericson, J., et al., 1997. Graded sonic hedgehog signaling and the specification of cell fate in the ventral neural tube. Cold Spring Harb Symp Quant Biol **62**, 451–466.
Briscoe, J., et al., 2000. A homeodomain protein code specifies progenitor cell identity and neuronal fate in the ventral neural tube. Cell **101** (4), 435–445.
Briscoe, J., et al., 1999. Homeobox gene Nkx2.2 and specification of neuronal identity by graded Sonic hedgehog signalling. Nature **398** (6728), 622–627.
Lu, Q.R., et al., 2000. Sonic hedgehog–regulated oligodendrocyte lineage genes encoding bHLH proteins in the mammalian central nervous system. Neuron **25** (2), 317–329.
Dessaud, E., et al., 2010. Dynamic assignment and maintenance of positional identity in the ventral neural tube by the morphogen sonic hedgehog. PLoS Biol **8** (6), e1000382.
Dessaud, E., et al., 2007. Interpretation of the sonic hedgehog morphogen gradient by a temporal adaptation mechanism. Nature **450** (7170), 717–720.
Ribes, V., et al., 2010. Distinct Sonic Hedgehog signaling dynamics specify floor plate and ventral neuronal progenitors in the vertebrate neural tube. Genes Dev **24** (11), 1186–1200.
Goodrich, L.V., et al., 1997. Altered neural cell fates and medulloblastoma in mouse patched mutants. Science **277** (5329), 1109–1113.
Shetty, A.C., et al., 2010. SeqAnt: a web service to rapidly identify and annotate DNA sequence variations. BMC Bioinformatics **11**, 471.
Horner, V.L., Caspary, T., 2011. Disrupted dorsal neural tube BMP signaling in the cilia mutant Arl13b hnn stems from abnormal Shh signaling. Dev Biol **355** (1), 43–54.
Caspary, T., Larkins, C.E., Anderson, K.V., 2007. The graded response to Sonic Hedgehog depends on cilia architecture. Dev Cell **12** (5), 767–778.
Shen, J., et al., 1997. Skeletal and CNS defects in Presenilin-1-deficient mice. Cell **89** (4), 629–639.
Mariani, L.E., et al., 2016. Arl13b regulates Shh signaling from both inside and outside the cilium. Mol Biol Cell, pii: mbc.E16-03-0189.
Larkins, C.E., et al., 2011. Arl13b regulates ciliogenesis and the dynamic localization of Shh signaling proteins. Mol Biol Cell **22** (23), 4694–4703.
Pettersen, E.F., et al., 2004. UCSF Chimera–a visualization system for exploratory research and analysis. J Comput Chem **25** (13), 1605–1612.
Wang, C., et al., 2014. Structural basis for Smoothened receptor modulation and chemoresistance to anticancer drugs. Nat Commun **5**, 4355.
Kasarskis, A., Manova, K., Anderson, K.V., 1998. A phenotype-based screen for embryonic lethal mutations in the mouse. Proc Natl Acad Sci U S A **95** (13), 7485–7490.
Scherz, P.J., et al., 2007. Extended exposure to Sonic hedgehog is required for patterning the posterior digits of the vertebrate limb. Dev Biol **308** (2), 343–354.
Wang, C., et al., 2013. Structure of the human smoothened receptor bound to an antitumour agent. Nature **497** (7449), 338–343.
Byrne, E.F.X., et al., 2016. Structural basis of Smoothened regulation by its extracellular domains. Nature **535** (7613), 517–522.
Chen, J.K., et al., 2002. Inhibition of Hedgehog signaling by direct binding of cyclopamine to Smoothened. Genes Dev **16** (21), 2743–2748.
Ding, Q., et al., 1998. Diminished Sonic hedgehog signaling and lack of floor plate differentiation in Gli2 mutant mice. Development **125** (14), 2533–2543.
Matise, M.P., et al., 1998. Gli2 is required for induction of floor plate and adjacent cells, but not most ventral neurons in the mouse central nervous system. Development **125** (15), 2759–2770.
Mo, R., et al., 1997. Specific and redundant functions of Gli2 and Gli3 zinc finger genes in skeletal patterning and development. Development **124** (1), 113–123.
Fan, C.W., et al., 2014. The Hedgehog pathway effector smoothened exhibits signaling competency in the absence of ciliary accumulation. Chem Biol **21** (12), 1680–1689.
Jung, B., et al., 2016. Pitchfork and Gprasp2 Target Smoothened to the Primary Cilium for Hedgehog Pathway Activation. PLoS One **11** (2), e0149477.
Goetz, S.C., Anderson, K.V., 2010. The primary cilium: a signalling centre during vertebrate development. Nat Rev Genet **11** (5), 331–344.
Huangfu, D., Anderson, K.V., 2006. Signaling from Smo to Ci/Gli: conservation and divergence of Hedgehog pathways from Drosophila to vertebrates. Development **133** (1), 3–14.